JOURNAL OF Materials CHEMISTRY

The 63 K phase transition of $ZrTe_3$: a neutron diffraction study

Ram Seshadri,[a] Emmanuelle Suard,[b] Claudia Felser,[a] E. Wolfgang Finckh,[a] Antoine Maignan[c] and Wolfgang Tremel*[a]

[a]*Institut für Anorganische Chemie und Analytische Chemie, Johannes Gutenberg-Universität, Becher Weg 24, D-55099, Mainz, Germany*
[b]*Institut Laue Langevin, Avenue des Martyrs, BP156, Grenoble F-38042, France*
[c]*Laboratoire CRISMAT, ISMRA, 6, Boulevard Maréchal Juin, Caen F-14050, France*

Received 13th July 1998, Accepted 9th September 1998

The 63 K phase transition of $ZrTe_3$ has been followed through SQUID magnetisation and neutron diffraction studies. The transition is characterized by a small quenching of the magnetic susceptibility. Contrary to the expectation that the structural transition is associated with a charge density wave, the results of Rietveld refinements of high resolution neutron powder diffraction profiles indicate that below the phase transition the different bonding Te–Te contacts are more equal rather than less. The results are examined with the help of band structure calculations on structures determined at three different temperatures. The picture that emerges supports the view that anion–cation redox competition plays a crucial role in determining not only the structures of these compounds, but also the temperature dependence thereof.

Before the realization of high-T_c superconductivity in the layered copper oxides, considerable attention was paid to the physical properties of layered transition metal chalcogenides, in particular to the occurrence of phase transitions in systems such as $NbSe_3$ associated with the formation of charge density waves (CDW).[1] Of these chalcogenides, $ZrTe_3$ has had a rather colourful history. First reported by McTaggart and Wadsley,[2] the structure was determined by Furuseth *et al.*[3] who found for MX_3 (M = Ti, Zr, Hf and X = S, Se, Te) two different structure types within the $P2_1/m$ space group. In both structure types, the atoms occupy the 2(*e*) position (x, $\frac{1}{4}$, z). The atom positions of the so-called types A and B structures are related to one another through $x_A = 1 - x_B$ and $z_A = z_B$ for all the atoms. $ZrTe_3$ was determined as crystallizing in the type B structure.

Room-temperature resistivity measurements on $ZrTe_3$ suggested that it is metallic or semimetallic.[2] This was confirmed by Bayliss and Liang who performed optical reflectivity measurements on single crystals[4] and found that although the material is anisotropic, the strengths of the optical transitions along the different crystallographic directions are similar. Takahashi *et al.*[5] reported transport measurements on single crystals as a function of temperature. They observed an anomaly in the resistivity peaking around 55 K. The magnitude of the Hall coefficient was found to rise sharply at this temperature. Their initial interpretation was that the anomaly was caused by increased scattering of charge carriers rather than a decrease in their density. Below 2 K they found that $ZrTe_3$ becomes superconducting. These authors extended their first study, using elastic measurements to complement the transport studies.[6] While they could confirm the presence of the transition at 63 K, they were unable to establish whether it arose from a depletion of charge carriers or from increased scattering. The nature of the superconducting state turns out to be rather unusual, being described as not bulk, but filamentary from an analysis of the excess conductivity.[7] The nature of the transition associated with the resistivity anomaly was examined through electron diffraction and dark-field imaging at low temperatures by Wilson and coworkers,[8] who found that even at room temperature, some of the $ZrTe_3$ crystals displayed structural modulation. Below $\approx$ 63 K, they found a phase transition characterized by the appearance of superlattice spots at nearly $q = (\frac{1}{14}, 0, \frac{1}{3})$. Imaging in the satellite spots suggested that while along the a axis the structure has long-range coherence, there is considerable faulting along the other directions.

Canadell, Mathey and Whangbo[9] examined the electronic structure of type B $ZrTe_3$ in considerable detail within the extended Hückel approximation. They were interested particularly in the difference between $ZrTe_3$ and other group IV trichalcogenides. They suggested that the unusual properties of $ZrTe_3$ including the transition at 63 K could be explained only within the B type structure. These conclusions have since been undermined in the light of Furuseth and Fjellvåg[10] redetermining the structure of $ZrTe_3$ and establishing that it is all or mostly type A and not type B. Recently, photoemission and thermopower measurements and detailed electronic structure calculations on type A $ZrTe_3$ have been presented.[11] Through the use of so-called frozen-phonon calculations, the importance of short Te–Te distances (and metrical changes thereof) in determining the shape of the Fermi surface and the number of states near the Fermi energy have been established.[11] Nearly simultaneously a redetermination of the type A structure and detailed *ab initio* band structure calculations have been presented by Stöwe and Wagner.[12] The conclusions reached by these authors largely coincide with those presented in ref. 11 regarding the rôle of the short Te–Te contacts in influencing the electronic properties of $ZrTe_3$.

In the absence of a description of the structure of $ZrTe_3$ below the transition, and in particular of an idea of what happens to the different distances between the atoms, the precise nature of the transition would remain a matter of speculation. To this end, we have examined the evolution of the structure of $ZrTe_3$ through the collection and analysis of powder neutron diffraction (PND) profiles. We present the rather surprising results here.

The occurrence of what seemed to be a CDW transition and superconductivity in the same compound has prompted our interest in $ZrTe_3$. These two different ground states are sometimes thought to arise from similar causes but are usually competing. Indeed, in ref. 11 it has been suggested that the structural transition and superconductivity are related to independent features of the band structure. An understanding of the relations between crystal and electronic structure and physical properties of systems such as $ZrTe_3$ could yield insights crucial to the preparation of new materials with interesting properties.

Experimental

Sample preparation

An approximately 15 g powder sample of $ZrTe_3$ was prepared by heating well ground, stoichiometric mixtures of the elements in a sealed, evacuated quartz glass ampoule at 973 K for three days. Longer heating times were avoided because an analysis of the relevant Ellingham diagrams showed that the thermodynamic product (in reaction with the walls of the quartz glass ampoule) would be oxides of zirconium. This rather mild heating protocol resulted in samples contaminated by small amounts of $ZrTe_5$ (determined from the PND profiles). The samples also suffered some texturing.

SQUID magnetisation

Magnetisation data under a 1 T field were collected on a 0.1174 g sample of $ZrTe_3$ on cooling between 100 and 5 K in a Quantum Design MPMS 5 magnetometer. The sample was held in a gelatine capsule that was fixed to the end of a drinking straw. The magnetisation of the gelatine capsule and drinking straw were recorded separately and fitted with high reliability to the analytic form $M=A_0+A_1/T$. This was then used to correct the data for the sample holder.

Neutron diffraction

Neutron data were collected on two different diffractometers, D2B and D20 at the Institute Laue-Langevin, Grenoble France. D2B is a high resolution diffractometer and as we shall see the resolution of the powder profiles obtained on it were largely sample limited. Data on D2B were collected at 1.7 and 100 K using a wavelength of 1.5941 Å. In order to enhance the resolution a 10′ primary beam collimation was employed and the monochromator beam divergence was limited by means of a system of slits positioned after the monochromator. The uncertainties in the temperature are throughout <0.2 K. Each data collection took about 12 h. D20 is a diffractometer of lower resolution but working with a fixed sample and detector. As a result, during an experiment (*e.g.* a temperature ramp) there are effectively no systematic errors introduced. The special geometry of D20 allows rapid acquisition of diffraction profiles of very low noise and very high precision both in counts and in scattering angle. We also attempted to study the pressure dependence of the structure of $ZrTe_3$ using a hydrostatic Ti–Zr ('zero matrix') pressure cell with He as the working fluid. Data were collected at fixed temperature while ramping the pressure up to 1000 bar. Due to certain experimental constraints, the data were of insufficient quality[13] for positional parameters to be extracted.

The data were analyzed using the Rietveld method[14] as implemented in the XND program.[15] We have used a special feature of this implementation which requires some explanation. When several diffraction profiles are collected as a function of some external variable (temperature, pressure, composition *etc.*), two possibilities exist for their treatment. The prevailing method is to refine each data set independently, extracting structural parameters that are then assembled in order to follow a certain trend. The lesser used alternative is implemented in the XND Rietveld program, allowing the refinable parameters in the structural model to be expanded as a polynomial in the external variable. This results in a considerable reduction in the ratio of refinable parameters to data, providing better refinements from data sets of limited quality. This has been previously employed to examine the composition dependence of structure in some layered manganites.[16]

The profiles are handled in the reciprocal space as convolutions of Lorentzian and Gaussian functions with their individual angular dependencies. Preferred orientation (particularly for the data acquired on the D20 diffractometer under pressure) was treated using first order Legendre polynomials to weight the calculated profiles in suitable reciprocal space directions. Asymmetry was handled using the Hermite polynomial approach of Bérar and Baldinozzi.[17]

During the later stages of the refinement, some peaks were found to be fitted rather poorly. Through trial and error, a small quantity of $ZrTe_5$[18] was found to be present in the sample. This phase was therefore included in all the refinements presented here. For the D20 diffractometer, the wavelength was calibrated to be 2.4085 Å using a yttrium iron garnet (YIG) standard, and for the D2B diffractometer the wavelength was calibrated to be 1.5941 Å using an Si standard.

Cell volumes and their errors were calculated using standard formulae.[19] Other metrical information was obtained through the use of the PLATON97 program.[20] Correlations between the different refined parameters were ignored in the calculations of quantities such as interatomic distances and angles.

Band structure calculations

The electronic structure of type A $ZrTe_3$ has been discussed in detail in ref. 11 and is discussed only very briefly here. Tight-binding linear muffin-tin orbital (LMTO) band structure methods[21] were used within the atomic sphere approximation (ASA). The calculations were performed on the room-temperature single crystal X-ray structure of Furuseth and Fjellvåg[10] and the structures obtained from the Rietveld refinement of the D2B data at 100 and 1.7 K. 2774 irreducible k points were used to achieve convergence.

Results and discussion

Description of type A $ZrTe_3$

Despite it having been discussed extensively in the literature,[3,9,11,22] we present for completion a depiction of the structure of type A $ZrTe_3$ in the panels of Fig. 1 focusing on those aspects of the structure that we will find most important with respect to the phase transition. The Zr atoms are eight-

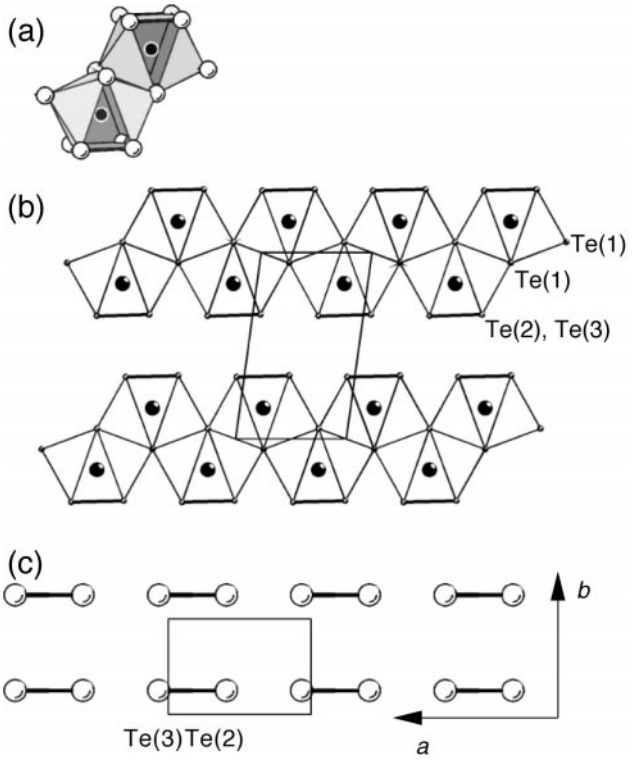

Fig. 1 Structure of type A-$ZrTe_3$ showing (a) the nature of the Zr–Te polyhedra, (b) the complete structure projected down [010] with the Te atoms marked and (c) the nature of the Te(2)–Te(3) contacts within the sheets.

coordinated by Te as shown in Fig. 1(a). These polyhedra are arranged in double sheets stacked along the monoclinic c axis as displayed in Fig. 1(b), where the view is looking down [010]. The basal plane is then defined by rectangular sheets of Te(2) and Te(3) atoms with short and long distances between them as shown in Fig. 1(c) (with a view down [001]). The Te(1) are arranged in buckled sheets around $z=0$ and $z=1$. Sheets of Zr are then stacked between the Te sheets in a manner that yields the coordination depicted in Fig. 1(b). The motif of rectangular sheets, with short, alternating Te(2)–Te(3) contacts along the a direction is something that we return to in the discussion of the phase transition. Note that when presented in the manner employed here the structure of $ZrTe_3$ is very much quasi-2D, comprising slabs that are stacked along the monoclinic c axis. We prefer this description over the traditional view that the structure is quasi-1D or chain-derived.

Magnetic susceptibility

Between 100 and 65 K, the SQUID susceptibility (corrected for sample holder contribution and for core diamagnetism[23]) displayed in Fig. 2 is effectively Curie–Weiss. Below this temperature, the susceptibility and its inverse display a small plateau, before once again reverting to nearly Curie–Weiss behaviour around 30 K. The phase transition can thus be described as a small quenching of the susceptibility. We postpone the interpretation of this behaviour to after we have discussed the structure. The CDW transition in $ZrTe_5$ takes place above 100 K,[24] so the changes observed here cannot be attributed to the small amount of the $ZrTe_5$ impurity that is present.

Thermal evolution of the structure

We commence with a description of the evolution of the cell volume between 120 and 1.9 K. The D20 data were collected on a continuous temperature ramp from 1.9 to 200 K with data being binned into approximately 4 K intervals. The refinements yielded the cell volume evolution displayed in Fig. 3 as small filled circles with error bars. The squares at 1.7 and 100 K are from refinements of the high resolution D2B data discussed shortly. The error bars for these two data are smaller than the symbols (note that at 1.7 K, the points from D2B and D20 overlap). Between 120 and 65 K, the data can be fitted with high reliability to a straight line. The data point at 61 K deviates significantly from this evolution. Between 61 and 13 K, the volume evolves in a nearly quadratic manner as shown by the fitted curve. The fits allow the transition to be characterized by a *very* small volume contraction at 63 K of about 0.02%.

The evolution of the individual lattice parameters with temperature is displayed in the different panels of Fig. 4. We observe immediately that the clearest changes are along the a axis. From the preceding discussion of the structure, this would implicate the Te(2)–Te(3) distances in the phase transition. The points with error bars are the values obtained from individual Rietveld refinements of D20 data. The lines are the results of refinement of two structural models against 13 data sets above the transition and (separately) against 13 data sets below the transition, expanding all refineable structural parameters to first order in the temperature. More explicitly, instead of refining some structural parameter p, the parameter is expanded in the temperature according to $p=p_0+p_1(T)$. p_0 and p_1 are then refined against N data sets acquired at the different temperatures T. At the end of the refinements, one obtains p_0, p_1, and the errors dp_0 and dp_1. The close correspondence between the points from individual refinements and lines

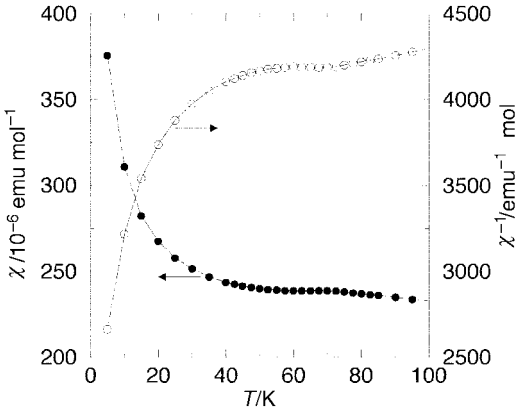

Fig. 2 Temperature dependence of the magnetic susceptibility and its inverse of $ZrTe_3$ under a 1 T magnetic field. The lines are guides to the eye.

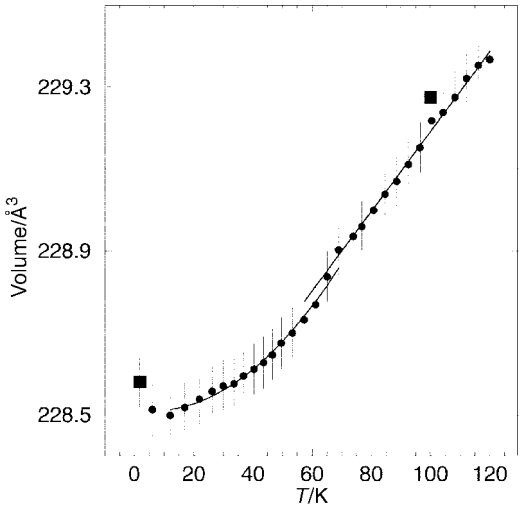

Fig. 3 Temperature dependence of the unit cell volume of $ZrTe_3$ as a function of temperature. The filled circles are D20 data and the squares are D2B data. For the D2B data, the error bars are smaller than the symbols. The solid line is a linear fit to data above 63 K and the curve is a quadratic fit to the data between 13 and 61 K.

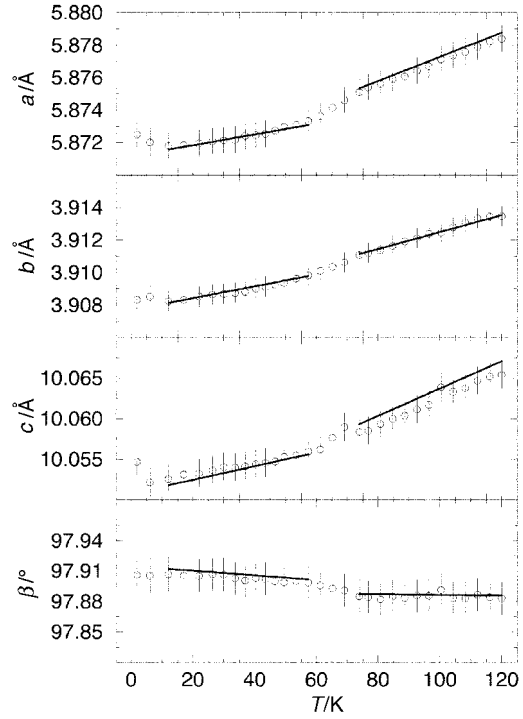

Fig. 4 Temperature dependence of the cell parameters of $ZrTe_3$. The points with error bars are from individual refinements of D20 data and the lines are from coupled refinements of D20 data (13 data sets at a time) treated separately above and below the transition.

obtained from the coupled refinements validates the procedure (and especially, the first order expansion). The necessity for this coupling is that the structural parameters thus obtained are of greater reliability, possessing smaller error bars. Methods for estimating the error from such a coupled refinement have been presented previously.[16,25] In the present case they are approximately half as small as the error bars associated with the parameters resulting from refining the data sets individually. Since the strategy of the coupled refinements yields a temperature dependence of structure (*i.e.* a state function rather than a state point), we can calculate the different structural parameters at arbitrary temperatures within the refined state function. Doing so at the temperatures of 50 and 80 K, representing the structure below and above the phase transition, we obtain the distances presented in Table 1. The magnitudes of the error bars in this table are clearly too large to discern changes in interatomic distances that might characterize the phase transition. We note however, that the long and short Te(2)–Te(3) distances are 2.99(5) and 2.88(5) Å at 50 K while they are 3.00(9) and 2.88(9) Å at 80 K. The D20 data thus do not support the traditional picture of a CDW transition, following which one would expect a divergence in the distances below the transition.

Structures at higher resolution

Refinement of data from the D2B diffractometer at temperatures around 100 K and 1.7 K yield structures of much higher precision. Fig. 5 displays the experimental and fitted PND (D2B) profile of $ZrTe_3$ (with a small $ZrTe_5$ admixture) collected at 1.7(1) K. The fit between the data and the refined model is not very good, due to problems of texturing in the sample, and what seems to be high dispersion in the structural coherence lengths in the sample. This is also manifested in the rather large values of the agreement factors; the Bragg and weighted profile R factors. Indeed, refining two $ZrTe_3$ phases with all structural parameters except the lattice parameters constrained, and allowing for different peak widths corresponding to distinct particle sizes did result in better fits (lower weighted-profile R factors) but considerably increased the number of refined parameters, leading us to abandon this strategy. Nonetheless, the errors on the interatomic distances seem to be only slightly larger than those associated with the high-quality single-crystal results presented in ref. 10. From the refined Rietveld scale factors, quantitative analysis[26] ignoring the Brindley factors[27] (which are not very important for neutron refinements) suggested that the $ZrTe_5$ impurity included in all the refinements presented here was as high as 15%. Table 2 lists the structural parameters of $ZrTe_3$ obtained from the refinements at the two temperatures, and Table 3, the important interatomic distances extracted from the data. For comparison, interatomic distances obtained in the room-temperature single-crystal study of Furuseth and Fjellvåg[10] are also displayed. The most significant differences between the structures at the three temperatures are in the short and long Te(2) and Te(3) distances, which show a small but perceptible divergence between 1.7 and 100 K, through to the room temperature. This is plotted in Fig. 6. If the structural changes at 63 K were associated with a CDW-like distortion of the sheets defined by Te(2) and Te(3), the observed metrical behaviour is precisely the opposite of what would then be expected.

Table 1 Interatomic distances obtained from the coupled Rietveld refinement of D20 data, calculated at 50 and 80 K

Atom 1	Atom 2	D(50 K)/Å	D(80 K)/Å
Te(1)	Zr	3.09(4)	3.08(7)
Te(1)	Zr	3.13(4)	3.14(7)
Te(1)	Zr(×2)	2.97(3)	3.01(5)
Te(2)	Zr(×2)	2.98(3)	2.96(6)
Te(3)	Zr(×2)	3.01(3)	3.01(5)
Te(2)	Te(3)	2.88(5)	2.88(9)
Te(2)	Te(3)	2.99(5)	3.00(9)

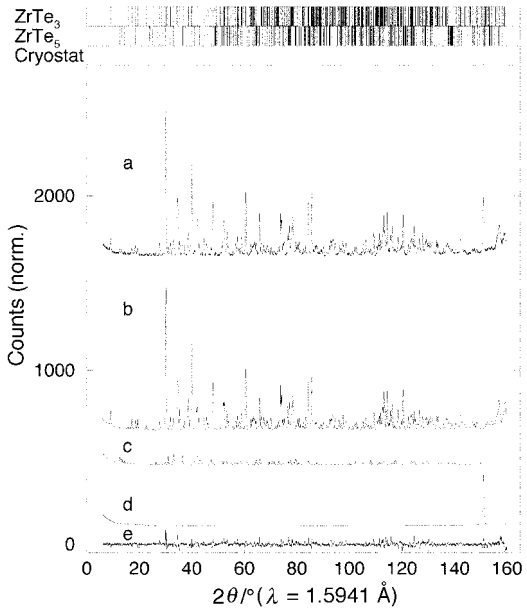

Fig. 5 Rietveld refinement of D2B data acquired at 1.7(1) K. The data (a), Rietveld fit to the $ZrTe_3$ structure (b), Rietveld fit to the $ZrTe_5$ structure (c), a parasitic peak due to the cryostat (d) and the difference between observed and refined profiles (e) are displayed, as are markers of the peak positions for the different structures.

Densities of state and the nature of the transition

In Fig. 7 we display a comparison of the Te(2) and Te(3) p-orbital and Zr d-orbital derived densities of state (DOS)

Table 2 Structures obtained from the Rietveld refinement of D2B data at 1.7 and 100 K. Space group $P2_1/m$ (no. 11)

Atom	x	y	z	B/Å^2
$T = 1.7$ K[a]				
Zr	0.2878(4)	0.25	0.6654(3)	0.84(5)
Te(1)	0.7635(6)	0.25	0.5574(2)	0.73(6)
Te(2)	0.4284(5)	0.25	0.1647(3)	0.08(5)
Te(3)	0.9068(6)	0.25	0.1600(3)	0.24(5)
$T = 100.0$ K[b]				
Zr	0.2882(5)	0.25	0.6648(3)	1.00(5)
Te(1)	0.7643(6)	0.25	0.5579(3)	0.84(6)
Te(2)	0.4297(5)	0.25	0.1650(3)	0.25(5)
Te(3)	0.9068(6)	0.25	0.1601(3)	0.46(5)

[a] $a = 5.8726(3)$, $b = 3.9084(2)$, $c = 10.0536(5)$Å, $\beta = 97.848(3)°$. $R_B = 9.7\%$, $R_{wp} = 8.5\%$. [b] $a = 5.8775(3)$, $b = 3.9125(2)$, $c = 10.0645(5)$Å, $\beta = 97.835(3)°$. $R_B = 9.4\%$, $R_{wp} = 8.2\%$.

Table 3 Interatomic distances obtained from the Rietveld refinement of D2B data, at 1.7 and 100 K, compared with those at 298 K

Atom 1	Atom 2	D(1.7 K)/Å	D(100 K)/Å	D^a(298 K)/Å
Te(1)	Zr	3.132(4)	3.132(5)	3.156(2)
Te(1)	Zr	3.122(4)	3.120(5)	3.140(2)
Te(1)	Zr(×2)	2.957(3)	2.959(3)	2.956(1)
Te(2)	Zr(×2)	2.956(3)	2.956(3)	2.939(2)
Te(3)	Zr(×2)	2.959(3)	2.966(3)	2.961(2)
Te(2)	Te(3)	2.816(5)	2.811(5)	2.793(2)
Te(2)	Te(3)	3.057(5)	3.067(5)	3.103(2)

[a] Single crystal data of Furuseth and Fjellvåg.[10]

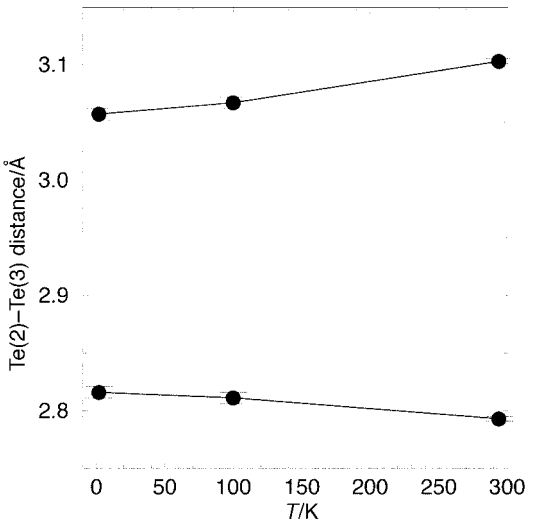

Fig. 6 Evolution of the short and long Te(2)–Te(3) distances with temperature. The 298 K data are from the single crystal study of Furuseth and Fjellvåg.[10]

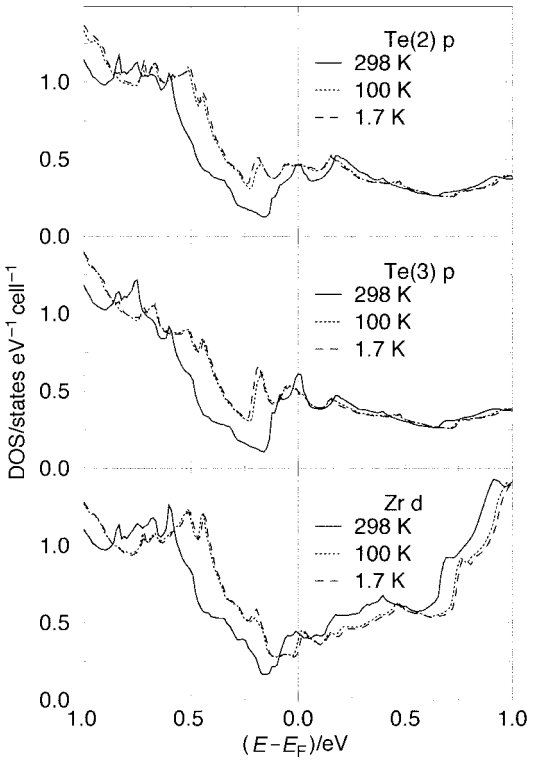

Fig. 7 Partial LMTO densities of state of $ZrTe_3$ calculated using the published 298 K structure of Furuseth and Fjellvåg[10] and the structures determined in this study at 100(1) and 1.7(1) K. The Te(2)-p, Te(3)-p and Zr-d states are shown in a small window around the Fermi energy.

obtained from high level LMTO calculations on the structures at three different temperatures. Without going into the details of the electronic structure (discussed extensively in ref. 11), we note that the Te(2)–Te(3) p-orbital interaction is σ*, and this interaction results in a partially filled band that crosses the Fermi energy. Changing the distances between the Te(2) and Te(3) atoms in the sheets should result in some rearrangement in the number of states in the valence band. In fact, the photoemission data (acquired at 298 and 80 K) presented in ref. 11 support the picture of a transfer of weight from the valence band to just below E_F, in keeping with what is observed here. The structural transition is thus associated with a rearrangement of some states arising from (or causing) changes in Te(2)–Te(3) distances. More simply, the transition is associated with charge transfer.

Rouxel has argued eloquently for the importance of what he calls redox-competition[28] in going from oxides to the more covalent transition metal chalcogenides, whereby the observed reduction in the energy difference between cation d bands and anion sp bands results in a competition between these for valence electrons. In the previous work from this group[11] the importance of such redox competition in the $ZrTe_3$ system was discussed. Access to the low-temperature structures now allows us to show that redox competition not only governs structural principles but perhaps also the temperature dependence thereof.

The changes in the DOS indicate that the biggest differences occur between the room temperature and 100 K rather than between 100 and 1.7 K as one might expect from the temperature at which the transition is found. However, the band structure calculations are effectively at 0 K, and the rôle of phonons is ignored. It is possible that when temperature effects are taken into account, the situation would correspond more closely to what is observed. We interpret the quenching of the magnetic susceptibility as arising from a small decrease in the total density of states (not shown) at the E_F on cooling below the transition temperature resulting in a decrease in the Pauli paramagnetic contribution. The sharp drop in the thermopower along the *a* axis at the transition and below[11] [the direction being that of the Te(2)–Te(3) contacts] could be ascribed to increased mobility along this axis.

The one question remaining seems to be the symmetry change at the phase transition associated with a structural modulation as observed in the electron diffraction measurements. Electron diffraction is much more sensitive to changes in symmetry than is powder neutron diffraction (particularly when the symmetry change is associated with a very large supercell) while it does not enjoy the metrical precision of neutron diffraction coupled with Rietveld refinement. Indeed, that the symmetry of the low-temperature structure could be different is suggested by the behaviour of the thermal parameters. Those of Zr and Te(1) at 1.7 K are about 80% the values at 100 K, but for Te(2) and Te(3) the changes in *B* on cooling are larger, the values of *B* at 1.7 K for Te(2) being about 30% of the value at 100 K and for Te(3) about 50% of the value at 100 K. The use of the $P2_1/m$ space group with its associated unit cell for the low-temperature refinement is thus only approximate, being the commensurate subcell of some lower symmetry system. We do not expect this to affect our conclusions regarding the trends in the interatomic distances.

The nature of the rearrangement of atoms within the sheets permits the classification of the transition as displacive and second order.[29,30] Identifying an order parameter in the structural metric from the present study is however made difficult by the fact that the Te–Te distances along the *a* axis are unequal in both the high and the low temperature phases. That the low-temperature structure [when we consider only the Te(2)–Te(3) sheet] is less distorted than the high-temperature structure is perhaps unusual but by no means novel. Perovskite manganites of the general formula $Ln_{1-x}A_xMnO_3$ where Ln is a rare-earth ion and A is an alkaline earth ion have received much recent attention because of the finding that in these systems the onset of ferromagnetism on cooling is accompanied by the phenomena of giant negative magnetoresistance (GMR) being displayed.[31] Careful structural investigations on such GMR manganites have revealed that the delocalization of the e_g electron on Mn^{III} below the ferromagnetic transition results in the MnO_6 octahedra being less distorted below the transition temperature rather than more.[32] Similar effects have been observed as a function of temperature or pressure in some layered manganites.[33] In $ZrTe_3$, the transition in the thermopower and the quenching

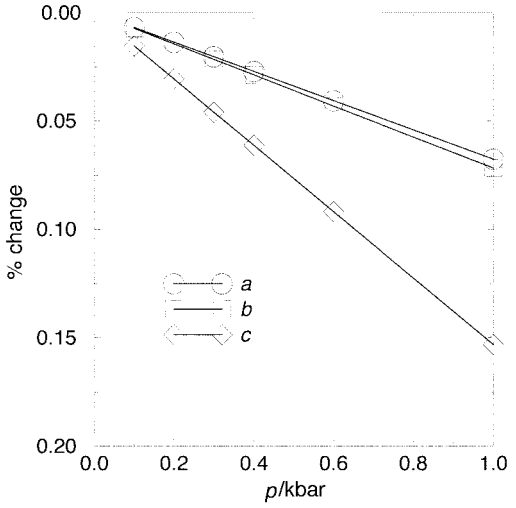

Fig. 8 Isothermal (19 K) pressure dependence of the *a*, *b* and *c* lattice parameters of $ZrTe_3$ obtained from a coupled refinement of D20 data during a pressure ramp from ambient pressure to 1 kbar.

of the susceptibility, in conjunction with the calculated decrease in the DOS at the E_F below the transition suggests that what is observed is similar to the situation in the manganites except that the the cause is not an atomic energy level (a Jahn–Teller distortion) but rather the behaviour of the σ* band formed by Te(2) and Te(3) p orbitals.

The effect of pressure on lattice parameters

From the discussion so far it is evident that only data of the highest quality can reveal details of the phase transition in $ZrTe_3$. From the isothermal data collected by us on the D20 diffractometer under pressure, it was not possible to extract structural parameters. However, through the use of the data-coupling strategy using six data sets, it was possible to obtain experimental compressibilities along the different directions. The assumption is that in the small pressure range studied (up to 1 kbar) the changes are linear. Fig. 8 displays the percentage changes in the *a*, *b* and *c* lattice parameters of $ZrTe_3$ at 19 K. The points refer to the temperatures at which the data were acquired. The error bars on the line are smaller than the points representing the temperatures. The Te(2)–Te(3) interactions along the *a* axes should be softer than the Zr–Te interactions so one might naïvely expect that this is the axis most sensitive to pressure. We find instead that both the *a* and the *b* axes have similar compressibilities but the *c* axis along which the sheets are stacked is significantly softer. This is in keeping with the presence of a van der Waals gap between the double sheets of the Zr–Te polyhedra and in keeping with the structural description that we have chosen. Similar results were observed from the pressure isotherms at 100 K suggesting that the transition seems to have no significant effect on the contractions of the different axes within the resolution of the experiment.

Acknowledgements

It is a pleasure to thank Professor O. K. Anderson and Dr. O. Jepsen for providing the LMTO codes, and Dr. P. Convert of the ILL for help and advice on D20. During the various stages of this work, we have received assistance from Dr. V. Ksenofontov and Mr. F. Rocker (Mainz) and Messrs. J. Torregrossa, L. Melesi and P. Cross (ILL). We thank them. This work has been supported by the Deutsche Forschungsgemeinschaft (DFG) and the Fonds der chemischen Industrie.

References

1 J. Rouxel, in *Crystal Chemistry and Properties of Materials with Quasi-One-Dimensional Structures*, ed. J. Rouxel, D. Riedel, Dordrecht, 1986 pp. 1–26.
2 F. K. McTaggart and A. D. Wadsley, *Aust. J. Chem.*, 1958, **11**, 845.
3 S. Furuseth, L. Brattas and A. Kjekshus, *Acta Chem. Scand. Ser. A*, 1975, **29**, 623.
4 S. C. Bayliss and W. Y. Liang, *J. Phys. C.*, 1981, **14**, L803.
5 S. Takahashi, T. Sambongi and S. Okada, *J. Phys. (Paris) Colloq. C*, 1983, **3**, 1733.
6 S. Takahashi, T. Sambongi, J. W. Brill and W. Roark, *Solid State Commun.*, 1984, **49**, 1031.
7 H. Nakajima, K. Nomura and T. Sambongi, *Physica B*, 1986, **143**, 240.
8 D. J. Eaglesham, J. W. Steeds and J. A. Wilson, *J. Phys. C.*, 1984, **17**, L697.
9 E. Canadell, Y. Mathey and M.-H. Whangbo, *J. Am. Chem. Soc.*, 1988, **110**, 104.
10 S. Furuseth and H. Fjellvåg, *Acta Chem. Scand., Ser. A*, 1991, **45**, 694.
11 C. Felser, E. W. Finckh, H. Kleinke, F. Rocker and W. Tremel, *J. Mater. Chem.*, 1998, **8**, 1787.
12 K. Stöwe and F. Wagner, *J. Solid State Chem.*, 1998, **138**, 160.
13 By quality, we refer to a combination of resolution, statistics (high signal to noise ratios) and dynamic range $s = \sin\theta/\lambda$ that would allow large numbers of parameters to be refined stably and with precision.
14 H. M. Rietveld, *J. Appl. Crystallogr.*, 1969, **2**, 5.
15 J.-F. Bérar, computer code XND version 1.11, ESRF, Grenoble, France, 1996; J. F. Bérar, Proceedings of the I.U.Cr. Satellite Meeting on Powder Diffraction, Toulouse, France, 1990; J. F. Bérar and F. Garnier, Advanced Powder Diffraction II Conference, N.I.S.T. Gaithersburg, Maryland, 1992; The program is freely available at the URL http://rx-crg1.polycnrs-gre.fr/public/xnd/xnd.html.
16 R. Seshadri, C. Martin, M. Hervieu, B. Raveau and C. N. R. Rao, *Chem. Mater.*, 1997, **9**, 270.
17 J.-F. Bérar and G. Baldinozzi, *J. Appl. Crystallogr.*, 1993, **26**, 128.
18 H. Fjellvåg and A. Kjekshus, *Solid State Commun.*, 1986, **60**, 91.
19 C. Giacovazzo in *Fundamentals of Crystallography*, ed. C. Giacovazzo, IUCr-Oxford, 1992, pp. 122–124.
20 A. L. Spek, computer code PLATON97, *Acta Crystallogr. Sect. A*, 1990, **46**, C34.
21 R. W. Tank, O. Jepsen, A. Burkhardt and O. K. Andersen, *The Stuttgart TB-LMTO-ASA program*, MPI für Festkörperforschung, Stuttgart, Germany, 1998.
22 W. Tremel and R. Hoffmann, *J. Am. Chem. Soc.*, 1987, **109**, 124.
23 K.-H. Hellwege and A. M. Hellwege, *Landolt-Börnstein Tables*, New Series, Volume 2, Springer-Verlag, Heidelberg, 1966; Note that the correction for core diamagnetism is considerably affected by how charges are assigned to the different atoms, so the true susceptibility might be in some error.
24 T. Sambongi, in *Crystal Chemistry and Properties of Materials with Quasi-One-Dimensional Structures*, ed. J. Rouxel, D. Riedel, Dordrecht, 1986 pp. 281–313.
25 Briefly, the final error on the refined parameter is independent of all terms except those that are of zeroth order in the expansion. For *N* parameters, we then have $dp = \sqrt{N} \times dp_0$. R. S. thanks Dr. J. P. Attfield for a clarification of this point.
26 J. Rodriguez-Carvajal, *Manual of the FullProf Rietveld Program*, Laboratoire Leon Brillouin, CEA Saclay, France, 1997. Available by anonymous ftp from bali.saclay.cea.fr.
27 G. W. Brindley, *Philos. Mag.*, 1945, **36**, 347.
28 J. Rouxel, *Chem. Eur. J.*, 1996, **2**, 1053.
29 H. D. Megaw, *Crystal Structures, A Working Approach*, W. B. Saunders, Philadelphia, 1973.
30 M. T. Dove, *Am. Mineral.*, 1997, **82**, 231.
31 C. N. R. Rao, A. K. Cheetham and R. Mahesh, *Chem. Mater.*, 1996, **8**, 2421.
32 V. Caignaert, E. Suard, A. Maignan, C. Simon and B. Raveau, *C. R. Acad. Sci. (Paris) Ser. IIb*, 1995, **321**, 515; P. G. Radaelli, M. Marezio, H. Y. Hwang, S. W. Cheong and B. Batlogg, *Phys. Rev. B*, 1996, **54**, 8992.
33 J. F. Mitchell, D. N. Argyriou, J. D. Jorgensen, D. G. Hinks, C. D. Potter and S. D. Bader, *Phys. Rev. B*, 1997, **55**, 63; D. N. Argyriou, J. F. Mitchell, J. B. Goodenough, O. Chmaissem, S. Short and J. D. Jorgensen, *Phys. Rev. Lett.*, 1997, **78**, 1568.

Paper 8/05427D